MFN= 007229
01 SID/SCD
02 5875
03 INPE-5875-PRE/2018
04 CEA
05 S
06 as
10 Scala, John R.
10 Garstang, Michael
10 Tao, Wei-Kuo
10 Pickering, Kenneth E.
10 Thompson, Anne M.
10 Simpson, Joanne
10 Kirchhoff, Volker Walter Johann Heinrich
10 Browell, Edward V.
10 Sachse, Glen W.
10 Torres, Arnold L.
10 Gregory, Gerald, L.
10 Rasmussen, R.A.
10 Khalil, M.A.K
12 Cloud draft structure and trace gas transport
14 17015-17030
30 Journal of Geophysical Research
31 95
32 D10
40 En
41 En
42 <E>
58 DGE/DIR
61 <PI>
64 Sept. <1990>
68 PRE
76 GEOFISICA ESPACIAL
83 Field observations obtained during the second NASA Amazon Boundary Layer Experiment (ABLE 2B), and two-dimensional moist cloud model simulations are used to determine the dominant transport pathways within a continental tropical squall line. A surface-based network triangle provided the focus for a multi-instrumental sampling of the May 6, 1987, squall line which propagated through the central Amazon basin at a rate of 40-50 km h-1. Extensive use is made of the vertical distribution of specific trace gases that are representative of the prestorm and poststorm environment. One-dimensional photochemical model results suggest the observed poststorm changes in ozone concentration can be attributed to convective transports rather than photochemical production. Two-dimensional cloud model results detail the dynamic and thermodynamic attributes of the simulated squall convection. The well-mixed moist troposphere in which the observed squall system developed may have hindered strong downdraft development. Parcel trajectory analyses are conducted to investigate the flow patterns of convective transports. A significant proportion (>50%) of the air transported to the anvil region originated at or above 6

km, not from the boundary layer via undilute cores. The presence of a midlevel inflow and a strong melting layer at 5.5 km reduced the vertical development of the core updraft and aided in the maintenance of a rotor circulation. The predicted absence of more than one active cell in the model cloud field, the lack of a well-organized downdraft in the presence of model estimated net upward mass flux, and the initial wind profile suggest the May 6 squall line was unicell in character.

90 b

91 FDB-19960401

92 FDB-MLR

JOURNAL OF GEOPHYSICAL RESEARCH, VOL. 95, NO. D10, PAGES 17,015–17,030, SEPTEMBER 20, 1990

Cloud Draft Structure and Trace Gas Transport

JOHN R. SCALA,[1,2] MICHAEL GARSTANG,[1] WEI-KUO TAO,[3] KENNETH E. PICKERING,[4] ANNE M. THOMPSON,[3] JOANNE SIMPSON,[3] VOLKER W. J. H. KIRCHHOFF,[5] EDWARD V. BROWELL,[6] GLEN W. SACHSE,[6] ARNOLD L. TORRES,[7] GERALD L. GREGORY,[6] R. A. RASMUSSEN,[8] AND M. A. K. KHALIL[8]

Field observations obtained during the second NASA Amazon Boundary Layer Experiment (ABLE 2B), and two-dimensional moist cloud model simulations are used to determine the dominant transport pathways within a continental tropical squall line. A surface-based network triangle provided the focus for a multi-instrumental sampling of the May 6, 1987, squall line which propagated through the central Amazon basin at a rate of 40–50 km h^{-1}. Extensive use is made of the vertical distribution of specific trace gases that are representative of the prestorm and poststorm environment. One-dimensional photochemical model results suggest the observed poststorm changes in ozone concentration can be attributed to convective transports rather than photochemical production. Two-dimensional cloud model results detail the dynamic and thermodynamic attributes of the simulated squall convection. The well-mixed moist troposphere in which the observed squall system developed may have hindered strong downdraft development. Parcel trajectory analyses are conducted to investigate the flow patterns of convective transports. A significant proportion (> 50%) of the air transported to the anvil region originated at or above 6 km, not from the boundary layer via undilute cores. The presence of a midlevel inflow and a strong melting layer at 5.5 km reduced the vertical development of the core updraft and aided in the maintenance of a rotor circulation. The predicted absence of more than one active cell in the model cloud field, the lack of a well-organized downdraft in the presence of model estimated net upward mass flux, and the initial wind profile suggest the May 6 squall line was unicell in character.

1. INTRODUCTION

Convective clouds play a recognized role in the vertical distribution of atmospheric trace constituents [e.g., *Dickerson et al.*, 1987; *Gidel*, 1983; *Greenhut*, 1986; *Chatfield and Crutzen*, 1984]. Vertical transport within convective systems may affect the long-range transport of pollutants, resulting in an additional impact on regional air quality [*Cho et al.*, 1984; *Lyons et al.*, 1986]. Downward transport of trace gases by cumulus cloud pumping has been shown to be as significant as upward [*Garstang et al.*, 1988].

In a study of the transport processes of nonprecipitating cumulus clouds, *Ching and Alkezweeny* [1986] concluded that active clouds performed vertical mixing of the boundary layer and overlying cloud layer by effectively venting mixed layer pollutants. Recent modeling studies utilizing inert tracers suggest tropospheric concentrations can be significantly modified by convection [*Lafore and Moncrieff*, 1989; *Raymond et al.*, 1989; *Pickering et al.*, 1989*a*, *b*, 1990; *Moncrieff*, 1989]. While these studies have provided more information on the chemical composition of the convective troposphere, detail on the dominant pathways within convective clouds where most of the transport is accomplished remain poorly understood.

Convective circulations comprising the vertical transport behavior of cumulus clouds are known to play an active role in boundary layer modification [*Echternacht and Garstang*, 1976], anvil formation [*Gamache and Houze*, 1982], downdraft initiation [*Zipser*, 1969, 1977], and delivery of precipitation to the surface [*Johnson*, 1976]. Trace gas distribution within the atmospheric column is determined, in part, by this draft interaction. Therefore the interpretation of a trace constituent's tropospheric profile in the presence of convection necessitates a clearer understanding of convective cloud parcel trajectories. Motions within a developing cloud are difficult to sample, thus, observations in close proximity to active convection and numerical model simulations are required to detail the internal draft structure.

Drawing upon the shape of developing cumulonimbus clouds, *Newton* [1966] inferred their associated draft structure. More recently, large field programs like the National Hail Research Experiment (NHRE) and the Cooperative Convective Precipitation Experiment (CCOPE) have afforded the opportunity to investigate motions within thunderstorms of the High Plains. In particular, the knowledge gained from the combined use of aircraft, surface mesonetworks, and weather radar have aided in delineating regions of inflow and outflow [*Foote and Fankhauser*, 1973], and deducing the kinematics and trajectory patterns within low-level downdrafts [*Knupp*, 1987]. Airflow structure in midlatitude severe storms continues to receive considerable attention with the implementation of Doppler radar [*Miller et al.*, 1988].

The unique linear symmetry of squall line convection has encouraged numerous two-dimensional (2-D) model simulation studies [e.g., *Schlesinger*, 1973; *Brown*, 1979; *Nicholls*, 1987; *Seitter and Kuo*, 1983; *Weisman et al.*, 1988;

[1]Department of Environmental Sciences, University of Virginia, Charlottesville.
[2]Now at NASA Goddard Space Flight Center, Greenbelt, Maryland.
[3]Laboratory for Atmospheres, NASA Goodard Space Flight Center, Greenbelt, Maryland.
[4]Applied Research Corporation, Landover, Maryland.
[5]Instituto de Pesquisas Espaciais, São José dos Campos, São Paulo, Brazil.
[6]NASA Langley Research Center, Hampton, Virginia.
[7]NASA Wallops Flight Facility, Wallops Island, Virginia.
[8]Institute of Atmospheric Sciences, Oregon Graduate Center, Beaverton.

Paper number 90JD00597.
0148-0227/90/90JD-00597$05.00

Moncrieff, 1978]. Specifically, some recent work investigated the importance of ice-phase microphysics [*Fovell and Ogura*, 1988; *Tao and Simpson*, 1989], and the role of the environmental wind profile [*Hane*, 1973; *Dudhia et al.*, 1987; *Nicholls et al.*, 1988] in the development and maintenance of squall systems. Three-dimensional modeling efforts of squall line convection have advanced the theory of prominent 2-D flow dynamics and also suggested more complex updraft-downdraft interactions, transport pathways, and mixing mechanisms [*Moncrieff and Miller*, 1976; *Nicholls and Weissbluth*, 1988; *Tao and Soong*, 1986].

The purpose of this study is to utilize meteorological observations, chemical measurements, and model simulations to interpret convective cloud draft structure and to advance our knowledge of its role in the transport and vertical distribution of trace gases. We will present the results of a two-dimensional time-dependent cloud model simulation of the May 6, 1987, squall system observed during the second Amazon Boundary Layer Experiment (ABLE 2B). The mesoscale convective system exhibited evidence for significant mid-level detrainment in addition to transports to anvil heights. Chemical measurements of O_3 and CO obtained in the convective environment are used to predict photochemical production within a processed troposphere and to corroborate the cloud model results.

2. EXPERIMENT DESIGN

Field observations for this study were obtained during ABLE 2B based in Manaus, Brazil, in April and May 1987. The ABLE series of experiments were designed to investigate the relationship between undisturbed tropical ecosystems and the composition of the global troposphere as part of a longer term study devoted to the chemistry of the boundary layer [*Harriss et al.*, 1988].

A mesoconvective scale triangle encompassing nearly 1000 km^2 of the rain forest provided the focus for ground-based data collection, aircraft-borne measurements, and remotely acquired radar and satellite imagery (Figure 1). The experiment design enabled collection of appropriately spaced, detailed measurements of convective activity within a simple, triangular volume, and provided a useful framework for the interpretation of regional atmospheric chemistry.

Four portable automated mesonet (PAM) stations mounted on 45-m towers (5 m above the forest canopy) measured horizontal wind velocity, temperature, humidity (wet bulb thermistor), pressure, and precipitation (0.25 mm resolution) every second and recorded the information as 1-min averages. Data acquired from the PAM stations were transmitted via satellite to the National Center for Atmospheric Research for quality checks and storage. A micrometeorological tower operated at Ducke Reserve provided fast-response temperature, humidity, and the three components of velocity within and above the forest canopy [*Fitzjarrald et al.*, 1988].

Ducke, Embrapa, and Carapanã served as rawinsonde launch sites. Four soundings were made daily from Ducke and Carapanã (1200, 1500, 1800, and 2100 UT) and six from Embrapa (0000, 1200, 1500, 1800, and 2100 UT), totaling 356 during the field program. The rawinsonde instrument recorded horizontal wind velocity, temperature, humidity, and pressure every 20 m. A total of 20 ozonesondes were also launched from Ducke during ABLE 2B. A complete description of the procedures, data acquired, and sounding schedule are given by *Kirchhoff et al.* [this issue].

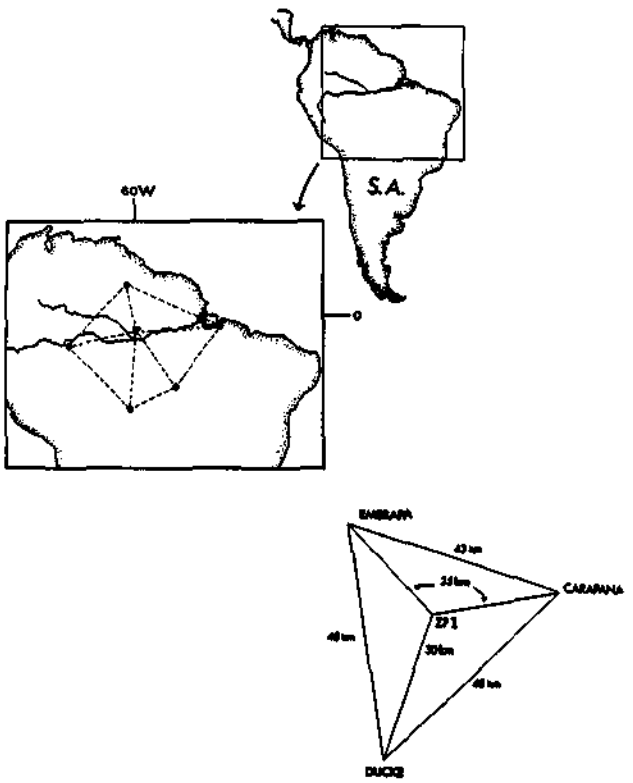

Fig. 1. The position of the ABLE 2B observation network (lower right) in the central Amazon Basin of South America is indicated by the solid triangle in the middle of the figure. The dashed polygon indicates the locations of the larger basin-scale rawinsonde network. Approximate dimensions and coordinates of the network triangle are also shown. PAM instruments are at Ducke, Embrapa, Carapanã, and ZF-1.

The NASA Wallops Electra aircraft was equipped with a range of chemical and meteorological instrumentation [*Garstang et al.*, 1989] to measure and characterize the lowest 5 km of the troposphere in the presence of developing convection. Performance limitations confined the Electra to the troposphere below 6 km. Aircraft missions were flown in conjunction with surface network operations. Of particular interest to this study is the downward and upward looking ultraviolet differential absorption lidar (UV-DIAL) which produces an uninterrupted vertical representation of aerosol and ozone content between the surface and the aircraft level of operation [*Browell et al.*, 1983]. More specific information on the airborne chemical measurements, including the acquisition of CO profiles, can be found in the work by *Harriss et al.* [1988].

Specific flight patterns were designed to couple airborne instrumentation with the surface based network in the presence of developing convective systems. Type of convection, location, and projected speed and direction of propagation determined the flight configuration (single wall, double wall, or volume). In the case presented here, the volume pattern was chosen to rapidly circumnavigate the surface network triangle at two levels (150 m and 3.5 km).

A computer directed 3-cm radar with volume scan capability and a 100-km effective range was used to document the

distribution, organization, speed of propagation, and echo development of convective systems in the vicinity of the network triangle. A 2-km constant altitude plan position indicator (CAPPI) was produced every 5 min as the instrument scanned through 12 successive levels. Quantitative estimates of rain rates could not be derived from the reflectivity fields due to signal attenuation.

Geostationary satellite coverage of the Amazon basin was utilized to determine the intensity, propagation, and development of convective systems which passed through the network triangle or were sampled by the aircraft. Full disk 4- and 8-km resolution visible and infrared images were available in addition to 2-km resolution imagery of the central Amazon Basin. The images were looped and animated during the field program through the use of a digital weather image data facility (DWIPS). This device conclusively determined the origin of the May 6, 1987, event to be along the northeast coast of Brazil.

3. SQUALL LINE OF MAY 6, 1987

The surface network observed 16 identifiable convective systems ranging in size and organization from weak lines to meso-scale complexes during the 45 days of wet season field operations. Several of these events were incompletely recorded due to instrument failure or lack of a scheduled aircraft flight. The squall line of May 6, 1987, was chosen for this study because of the near-complete sampling record by the surface-based network and the quality and content of the airborne measurements.

GOES imagery showed the convection associated with the May 6 squall line originated the previous day as a region of sea-breeze induced instability along the northeast coast of Brazil. A somewhat disorganized band of convection was established parallel to the coast by 0000 UT on May 6. During the next 10 hours, several areas of weak activity merged into three dominant clusters forming a linear arrangement as the system propagated to the southwest at a rate of 45 km h^{-1} (12.5 m s^{-1}) into the basin. The major components of the squall line continued to develop independently, clearly separated from each other by cloud-free air and still lacking a shared anvil at 1500 UT. The line elements reached maturity and merged after the system propagated through the network as evidenced by the formation of a well-glaciated, backward extending anvil region.

Although analysis of the 700-mbar wind field at 0000 UT on May 6 suggested diffluence in the region southeast of Manaus, speed convergence capable of supporting the squall convection did exist in the central basin. At 250 mbar, a line of convergence oriented northwest-southeast developed between Santarem (on the Amazon River, 600 km from the coast) and Belém (on the coast) by 0000 UT on May 6. An eastward shift in the position of the southern hemisphere subtropical anticyclone placed the circulation center over the southeastern coast of Brazil and adjacent western tropical Atlantic.

The leading convective elements of the squall line entered the northeastern portion of the surface network first at 1432 UT. Satellite imagery detailed the discontinuous nature of the convection that comprised the northwest-southeast line as it entered the triangle. Areas of deep convective activity were visibly separated by cloud-free, potentially outflow-modified air. As the squall line propagated through the instrumented region, more pronounced convection passed to the northwest and southeast. Embrapa recorded the most impressive gust front as the activity to the northwest apparently skirted that corner of the triangular network.

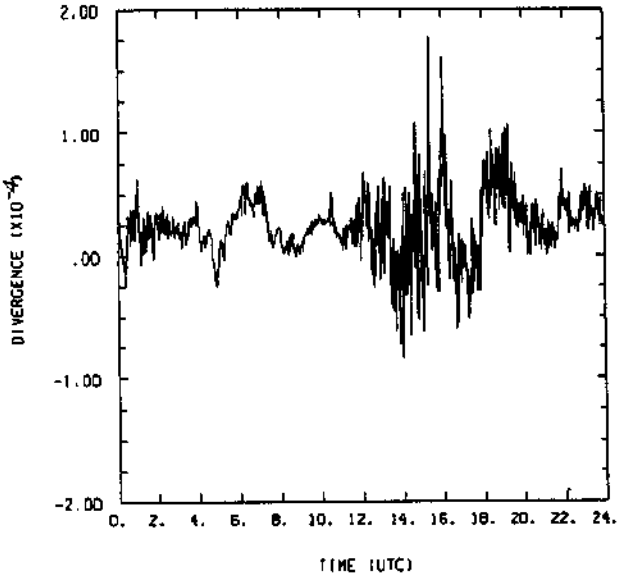

Fig. 2. The 24-hour surface network divergence for May 6, 1987, calculated from 1-min PAM wind averages. The units of divergence are 10^{-4} s^{-1}. The onset of diurnal heating, indicated by larger fluctuations in the wind field, is evident after 1000 UT.

Boundary layer convergence prior to passage of the squall line through the network was recorded by the PAM instrumentation atop the forest canopy. Surface divergence calculated every minute for May 6 placed this convective event in the context of daily wet season activity (Figure 2). Prior to the onset of surface heating, small amplitude fluctuations characterized the predominately divergent trend in the surface wind fields. Surface network convergence dominated at 1325 UT, prior to squall line passage, with peak convergence occurring about 60 min before Carapanã recorded a weak gust front. A second period of convergence after 1600 UT indicated the network response of a northwestward migrating outflow boundary through the network.

Gust front kinematics captured by the Embrapa PAM site are presented in Figure 3. The passage of the surface outflow boundary at 1520 UT is marked by a rapid drop in θ_e of 6 K and a marked wind speed (1-min average) maximum of 9 m s^{-1}. The resultant surface cold pool was not particularly impressive when compared with the 17 K drop in θ_e following the passage of April 26, 1987, storm outflow and gust front. An explanation for this relatively weak downdraft is presented in section 5.1. Rapid recovery of the boundary layer over the next 2.5 hours is clearly evident as θ_e returns to near-preevent values. The thermodynamic and kinematic sequence closely resembles signatures seen in surface fields in response to convective storms [*Burpee*, 1979; *Cooper et al.*, 1982; *Doneaud et al.*, 1984; *Ulanski and Garstang*, 1978; *Watson et al.*, 1981] with characteristic gradients in wind speed and temperature [*Charba*, 1974; *Wakimoto*, 1982; *Mahoney*, 1988].

The 2-km CAPPI shown in Figure 4 illustrates how well the echo field of the May 6 convective system was captured by the sampling network. A review of a sequence of radar

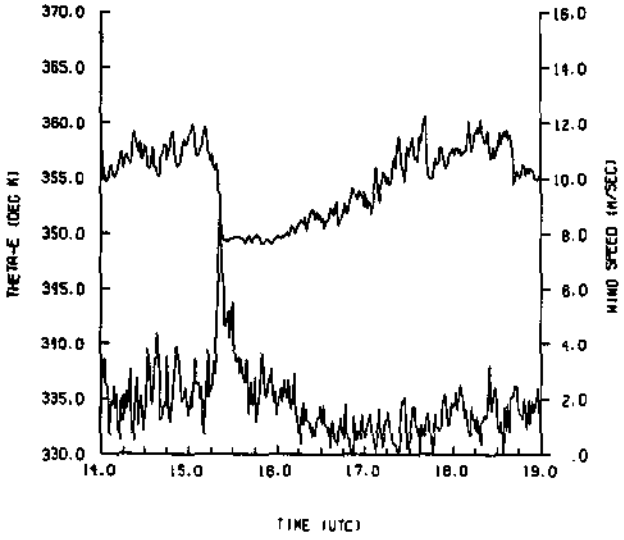

Fig. 3. Gust front passage at 1520 UT on May 6, 1987, recorded by the Embrapa PAM instruments. The upper trace is equivalent potential temperature, and the lower one is sustained horizontal wind speed (1-min average).

images which includes Figure 4 reveals a two-dimensionality to the convection that is observed in the satellite imagery but is not readily apparent in a single scan. The individual cells comprising the convection exhibit an east-west orientation within the overall linear organization. The sequence indicates the squall line maintained a southwest propagation through the network triangle.

Network divergence calculated in the presence of the convective cells presented in Figure 4 is assumed to be concentrated in the active cores of these cells. The shaded regions indicate high reflectivity gradients surrounding the core regions. Subcloud layer mass and moisture transports can be estimated from concurrent divergence calculations by utilizing these radar observed cores and employing an undilute draft from cloud base [*Garstang et al.*, 1989]. The shaded regions represent 39.0% of the echo field and 10.9% of the network area. Due to some attenuation of the radar signal, the reflectivity gradient is likely smoothed resulting in an overestimate of the area containing the centers of upward motion. The peak upward (3.9 m s^{-1}) and downward (1.9 m s^{-1}) vertical velocities calculated from divergences concentrated in these shaded regions produce moisture transports of 1.6×10^{10} kg and 7.6×10^{9} kg, respectively. These results compare favorably with subcloud moisture transports presented in other studies [*Braham*, 1952; *Auer and Marwitz*, 1968; *Foote and Fankhauser*, 1973; *Fankhauser*, 1988].

Aircraft circumnavigation of the network during the May 6 squall line passage provided a timely and unique perspective of this convective event. Following a carefully designed volume flight plan (Figure 5), the NASA Electra completed one full circuit at 3.6 km (requiring 20 min), spiraled down to 250 m, and completed a second circuit (requiring 22 min) prior to squall line advance into the triangle. The wind fields at these two levels combined with the surface PAM network

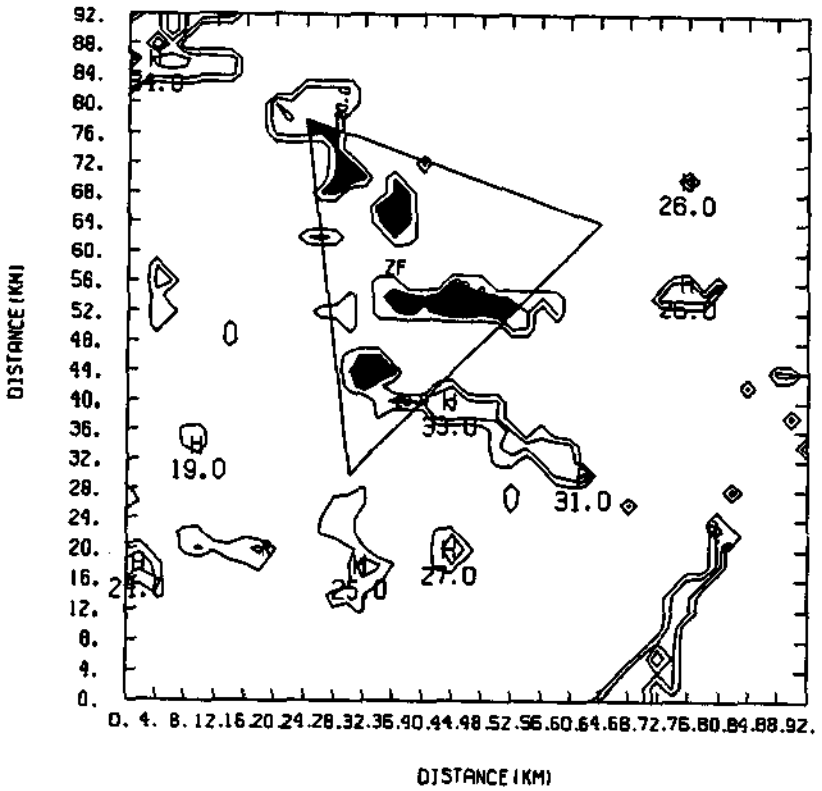

Fig. 4. Computer-derived 2-km CAPPI for 1527:58 UT observed by the ABLE 2B radar located at the Eduardo Gomes Airport, 15 km south-southwest of Ducke. The locations of the radar and the ZF-1 PAM site are denoted by the R and ZF, respectively. The contour interval of reflectivity is 10 dBz. The network triangle is the same as that in the lower right of Figure 1.

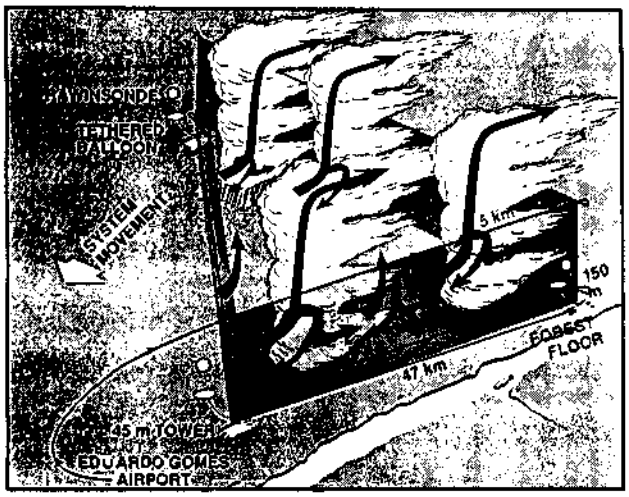

Fig. 5. Schematic representation of the "volume" aircraft mission flown to sample the convective environment of the May 6, 1987, squall line. The first volume enclosure (both upper and lower circuits) was completed in front of the line. The second captured the convection within the triangle. Ground-based measurement locations are shown at the network corners. The arrows are an artist's conception of the major inflow and outflow pathways relative to the convection, not May 6, 1987, specifically.

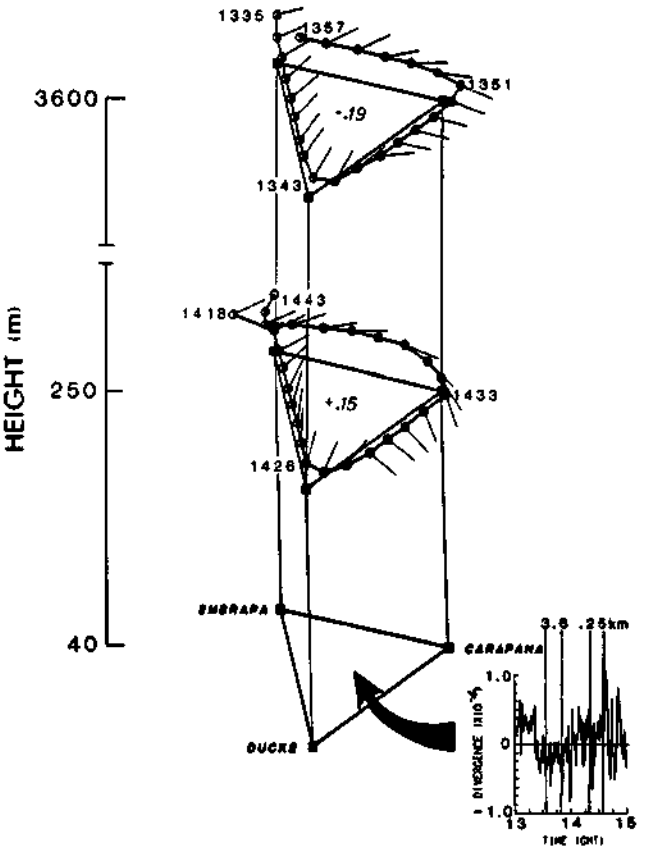

Fig. 6. Volumetric presentation of the calculated divergence fields obtained from the aircraft (flown at 3.6 and 0.25 km) and the surface-based PAM network. Aircraft observed wind fields are shown as barbs, indicating direction only. A time series of PAM divergence recorded while the aircraft completed the upper and lower patterns is located in the lower right with vertical lines indicating the aircraft sampling time at each level.

completed a volumetric coverage of the divergence fields through the column only minutes after outflows descending from the leading convective cells of the line impacted the triangle at 1437 UT (Figure 6). The PAM-derived divergence showed the aircraft did complete the upper and lower network circumnavigation in advance of the system.

The time series of surface divergence included in the lower right of Figure 6 shows that during the upper level circumnavigation (1335–1351 UT), both the PAM network and upper triangle were convergent. During the low-level circumnavigation (1418–1433 UT), and still prior to storm passage through the network triangle, both the surface and low-level aircraft winds indicated divergence. On the scale of the triangle, and in the presence of squall line cellular elements, both upward and downward motions were encountered in the time frame of 1 hour.

The integrated UV-DIAL ozone profile obtained in the wake region of the squall line is shown in Figure 7. The integration was evaluated over a time interval of just over 5 min (1725:30–1730:31 UT), corresponding to a flight distance of about 34 km. Unlike the dry season estimates of ozone in the lower troposphere [*Garstang et al.*, 1988], this profile, indicative of the more pronounced convection of the wet season, exhibits concentrations below 25 ppbv. A well-mixed layer is evident extending through cloud base into the lowest region of the cloud, and separated from another well-mixed layer above. A transition occurs between 2.25 and 2.8 km with substantial profile minimums at 2.2 and 3.2 km (which must be real compared to the estimate of error).

The vertical gradients of ozone observed in the vicinity of active convection can be used as evidence for local cloud scale draft transports [*Garstang et al.*, 1988]. The existence of vertical structure in Figure 7 is an unexpected result. We would expect to see vertical gradients of ozone from in situ measurements, but not from profiles obtained through horizontal integration where the cumulative effects of thorough mixing would be evident. These results suggest the presence of complex mixing in the low and middle levels as a consequence of deep convection.

An aircraft-derived vertical profile of CO, measured in situ in the wake of the convection contrasts sharply with the integrated O_3 profile (Figure 8). As evidence for upward mixing, boundary layer values are found in the midtroposphere despite the absence of structure in the profile. This single-location, single-profile measurement could be misinterpreted as representative of the wake region without the additional information provided by the net integrated O_3 data.

4. The Two-Dimensional Cloud Model

The two-dimensional moist cloud model used in this study is similar to that described by *Soong and Ogura* [1980], *Soong and Tao* [1980], *Tao and Soong* [1986], and *Tao and Simpson* [1989]. Several modifications to this nonhydrostatic and anelastic model, including microphysical processes, compressible system, lateral boundary condition, and stretched horizontal coordinate have been introduced. A parameterized three-category ice phase scheme (cloud ice, snow, and graupel) is included to augment a Kessler-type two-category liquid water scheme (cloud water and rain) for the model cloud microphysics. More than 27 different processes are included for computing the transfer rates between

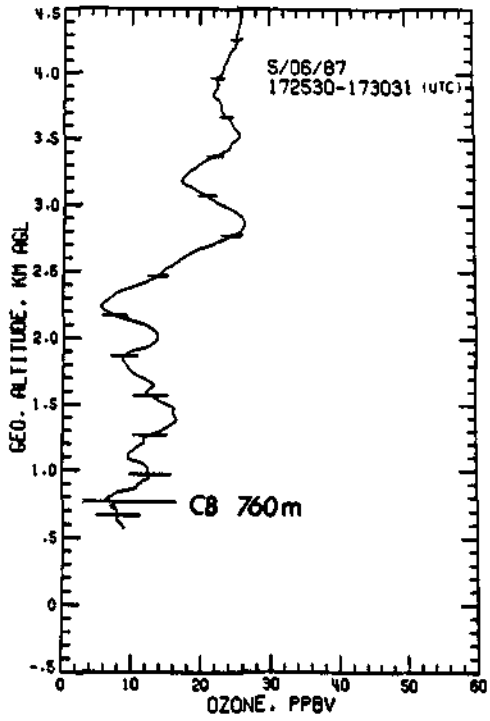

Fig. 7. Aircraft-derived horizontally integrated UV-DIAL profile of ozone (solid line) obtained in the wake of the squall line, 1725:30–1730:31 UT on May 6, 1987. Aircraft-observed cloud base at 760 m is included. The horizontal bars represent the standard error of the average mixing ratio for this portion of the flight. Despite a well-mixed lower troposphere, ozone concentration gradients are evident, representative of net cloud transport.

the hydrometeors. Recent tropical cloud system modeling efforts suggest the ice phase processes are essential for a realistic stratiform cloud simulation [*Tao and Simpson*, 1989].

A stretched vertical coordinate (incremental from 200 to 950 m) is used in order to maximize resolution in the lowest

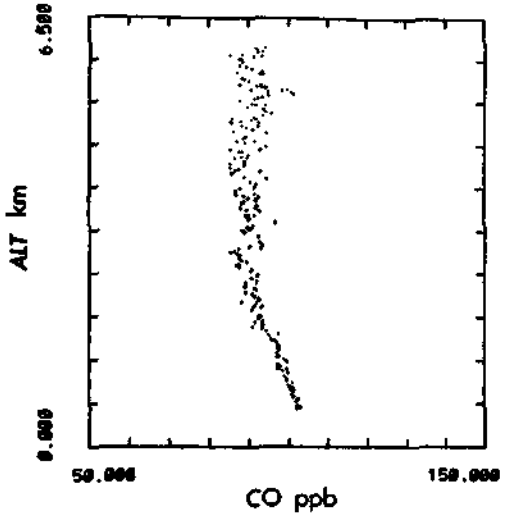

Fig. 8. Vertical profile of CO obtained during an aircraft spiral (1639:00–1714:00 UT) in the wake of the May 6, 1987, squall line. This single-point measurement reflects the net overturning and thorough mixing of the lower troposphere in the presence of convection.

levels of the model. Model top is 17.5 km with 31 grid points. The horizontal domain of the model contains 448 grid points. The central 368 comprise the fine grid area with a resolution of 500 m. The simulated cloud activity is confined to the fine resolution region through a Galilean transformation (by removing the 12 m s^{-1} propagation speed from the initial wind field). Outside of this region, the grid is also stretched with a ratio between grid spacings of 1.08:1. This results in a domain with a horizontal dimension of 464 km. An open lateral boundary condition [*Klemp and Wilhelmson*, 1978] is used along the x axis, parallel to the direction of squall propagation. The use of a stretched horizontal coordinate produces model results which are less sensitive to the choice of outward gravity wave speed [*Fovell and Ogura*, 1988].

Cloud scale motion is governed by a set of anelastic equations which only allow for gravity wave propagation. A leapfrog time integration and a second-order space derivative scheme are used. To avoid the problem of time splitting, a time smoother is adopted (Asslien filter). This smoothing coefficient is set to 0.1 using a time interval of 10 s. In general, each integration of the model covers an elapsed simulation time of 8 hours, requiring about 40 min of computer time on the NASA/GSFC Cyber 205. For a more specific description of the model attributes discussed here, the reader is encouraged to review the appropriate citations.

Wind and thermodynamic soundings from the network provided the initial conditions for the simulations (Figure 9). The pre-squall atmosphere (Figure 9*a*) was nearly saturated from the surface to 600 mbar. The large CAPE above cloud base (920 mbar) indicated the potential for deep convective development. The wind profile (Figure 9*b*) exhibits low-level shear below 2 km marked by relative inflow from the rear of the system. Relative weak midlevel inflow was present between 4 and 6 km, with stronger westerlies above that preventing the formation of a forward extending anvil. Figure 9*b* looks remarkably similar to the unicell wind profile discussed by *Dudhia et al.* [1987]. Repeated comparisons will be made between the kinematics of their simulated unicell convection and the May 6 squall system.

The convective cloud is initialized by a low-level cool pool maintained at a rate of -0.015°C s^{-1} over a 12-min period. The cool pool (6 km wide and 3 km deep) is placed close to the center of the model domain. A mesoscale upward motion with a peak magnitude of 2.3 cm s^{-1} at the 830-mbar level is superimposed (decreased to zero with height to 700 mbar). Only the base state thermodynamic field is adjusted by this imposed upward motion. This mesoscale lifting is assumed to be associated with a prestorm large-scale circulation typical of the tropics [*Tao and Soong*, 1986]. Through this arrangement, the initial thermodynamic sounding is destabilized, and the cloud develops. This forcing is only applied for the first 1 hour period; then it is decreased to zero by 2 hours simulation time.

5. Two-Dimensional Cloud Model Results and Discussion

5.1. *Cloud Fields*

Five two-dimensional simulations are required to reproduce the observed features of the convective system. Prior to each simulation, minor adjustments are made to the input variables (e.g., mesoscale forcing, strength of cool pool, thermodynamics) based on the results of the previous run.

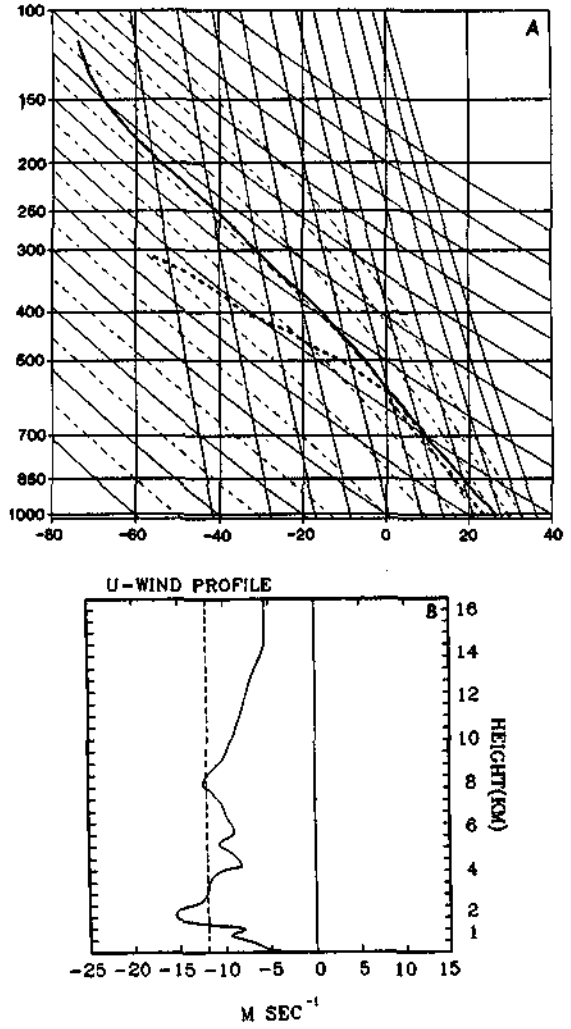

Fig. 9. Large-scale conditions used to initialize the cloud model simulations. (*a*) Composited profile of temperature and mixing ratio from 1500 UT Ducke and Carapanã rawinsoundings plotted for the presquall environment. (*b*) Wind component (u) normal to the leading edge of the squall line from the 1500 UT Carapanã wind profile. The dashed line represents the storm propagation speed.

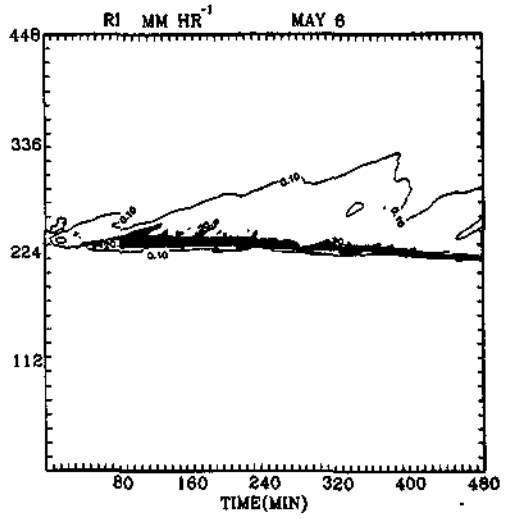

Fig. 10. Time evolution of the model-estimated surface rainfall rates for the 8-hour simulation. The shaded areas are considered to be convective in origin. The contour intervals are 0.1 and 20 mm h^{-1}.

The modifications improve specific attributes of the predicted cloud fields without altering the general structure and organization, which is accepted as the true behavior of the model cloud.

An x, p graphical representation of the model-calculated variables (which include horizontal and vertical velocities, temperature, and water vapor mixing ratio) is produced every 30 min during the 8-hour simulation. This time sequence of model-derived cloud fields enables an interpretation of convective updraft and downdraft development, cloud moisture content, surface precipitation structure, and modification of the initial atmosphere by the simulated cloud system.

The time evolution of estimated surface precipitation partitioned into convective and stratiform components is presented in Figure 10 for the entire 448 horizontal grid domain. The partitioning of squall line precipitation into convective and stratiform components follows the technique of *Adler and Negri* [1988]. The first 4 hours of the simulation are dominated by the growth of convective elements at the leading edge of the system and the production of convective rainfall. The second 4 hours are marked by growth of the anvil portion of the cloud and an associated areal increase in stratiform precipitation. One cloud system developed during the simulation and maintained a constant forward propagation.

The vertical cross section of model-predicted radar reflectivity at 360 min simulation time is presented in Figure 11. The 30 dBZ contour (heavy solid line) delineates convective precipitation at the leading edge and a decaying cell directly behind. The lowest reflectivity contour (10 dBZ) fails to indicate the formation of an anvil region. At 5.5 km, the melting of frozen meteors to rain is partly responsible for the bright band in the trailing stratiform region [*Tao and Simpson*, 1989].

Strong updrafts (9 m s^{-1} at 3 km) form only within the leading edge of the model cloud, suggesting the simulated convection is single or unicell in character (Figure 12). The

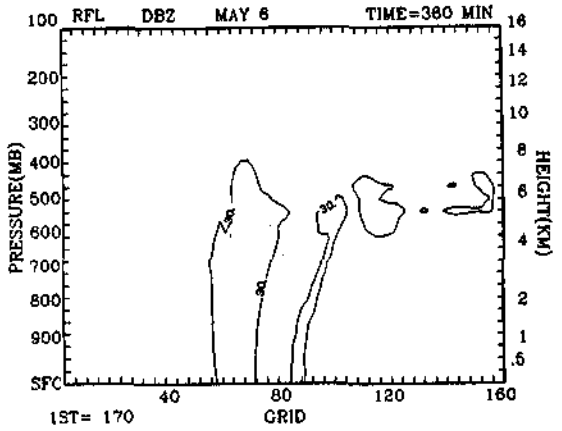

Fig. 11. Vertical cross section normal to the model squall system at 360 min of the simulation. The 30-dBz radar reflectivity contour (heavy solid line) delineates convective precipitation at the leading edge, a decaying cell directly behind, and a bright band near the freezing level within the stratiform region. The contour interval is 10 dBz. The horizontal dimension is 80 km.

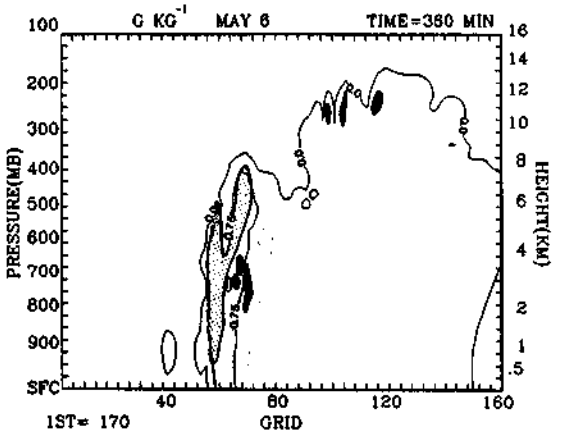

Fig. 12. Model-derived vertical velocity field superimposed on the model cloud outline at 360 min of the simulation. The cloud outline is based on total water content (cloud water, rain, ice, snow, and graupel). The contour interval is 0.25 g kg^{-1}. The hatched areas denote $w > 0.5$ m s^{-1}, and the dark areas $w < -0.5$ m s^{-1}.

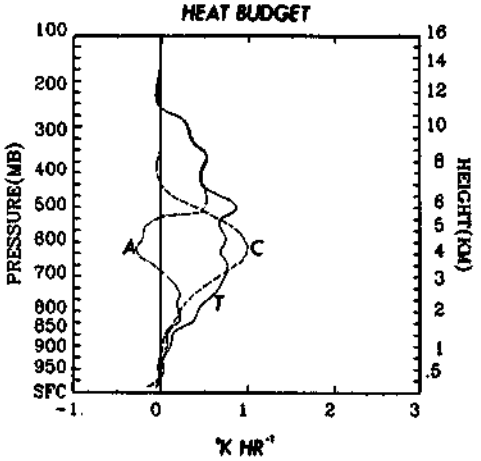

Fig. 14. Model-predicted heating budget profile for the second 4 hours of the simulation. The total heating (T) is partitioned into convective (C) and stratiform (A) components.

system propagates through the development and decay of convection at the front of the cloud, not by a density current sustained by strong outflows. Low-level convergence is apparently maintained by the lifting of boundary layer air at the leading edge of a propagating "solitary wave", a dynamical mechanism proposed by *Dudhia et al.* [1987] for the release of CAPE. The updrafts warm the local environment by 6 K between 2 and 8 km (Figure 13).

A portion of the updraft loses positive buoyancy and stops rising, thereby creating drag and initiating descent. The resulting downdraft is rather weak, cooling surface temperatures by only 2–3 K. Relatively cool and dry midtropospheric air necessary for efficient evaporation of precipitation and maintenance of strong downdrafts is absent. The thermodynamic outcome is minimal surface cooling by the simulated squall convection in agreement with the observations (Figure 3).

The vertical distribution of the column heating rates contributed by the convective and stratiform regions (Figure 14) reveals not only strong differences but an explanation for the lack of a dominant downdraft. Localized convective scale heating peaks near 625 mbar in response to an extremely moist sounding between 600 and 700 mbar. The stratiform (anvil) heating peaks near 375 mbar, where convective scale heating is negligible. The large predicted anvil heating is likely due to the inclusion of convective elements in the stratiform region by the model [*Tao and Simpson*, 1989]. This partitioning, however, does not alter the vertical distribution of total column heating. The anvil cooling peaks within a narrow region behind convective scale updrafts in the midtroposphere (650 mbar) due to melting of cloud ice and graupel. Little cooling by evaporation of rain is evident in the lower troposphere. By comparison, *Dudhia et al.* [1987] also found very small evaporation rates for their simulation of a unicell convective system. Thus mixing appears to play a more important role than evaporative cooling in determining the convective dynamics of this simulation.

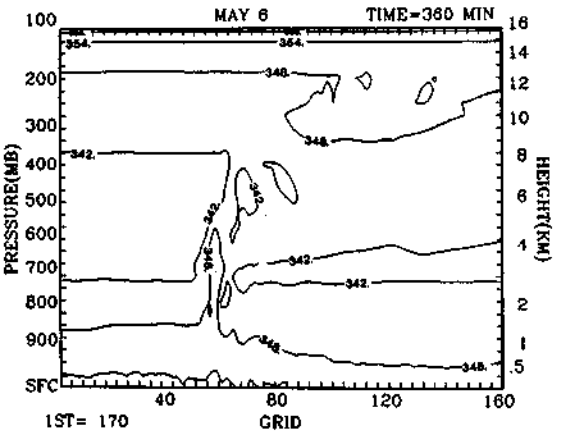

Fig. 13. Model-calculated equivalent potential temperature field at 360 min of the simulation. The contour interval is 2 K with dark solid lines every 6 K. The near-vertical updraft is easily discerned by the transport of 350 K air into the system.

The evidence for a well-mixed wet season troposphere over Amazonia can be seen in Figure 15. Average equivalent potential temperature profiles calculated from network raw-insoundings launched prior to and following the May 6 squall line are added to a figure compiled by *Aspliden* [1976], which presents a composite categorization of convection over Barbados in the tropical Atlantic. When compared with Aspliden's grouping of tropospheric conditions, the average wet season profiles plot further to the right than category VI (severely enhanced convection). The absence of a pronounced θ_e minimum in the low to middle troposphere may have hindered the development of strong downdrafts and prevented much cooler air from reaching the surface. The profiles presented in Figure 15 seem to imply that the *Riehl and Simpson* [1979] "hot tower" transport mechanism may not be necessary for vertical transport in regions of deep convection over the continental tropics. Instead, convection serves to thoroughly mix the troposphere, creating a condition where vertical transports can be efficiently accomplished by the mean Hadley/Walker circulations.

Several of the model results are supported by field observation and data analysis. Aircraft-derived profiles of ozone in the vicinity of deep convection on May 6 reveal vertical structure despite concentrations which average 50% lower than dry season estimates. The O_3 gradients are more indicative of local midtropospheric detrainment and mixing

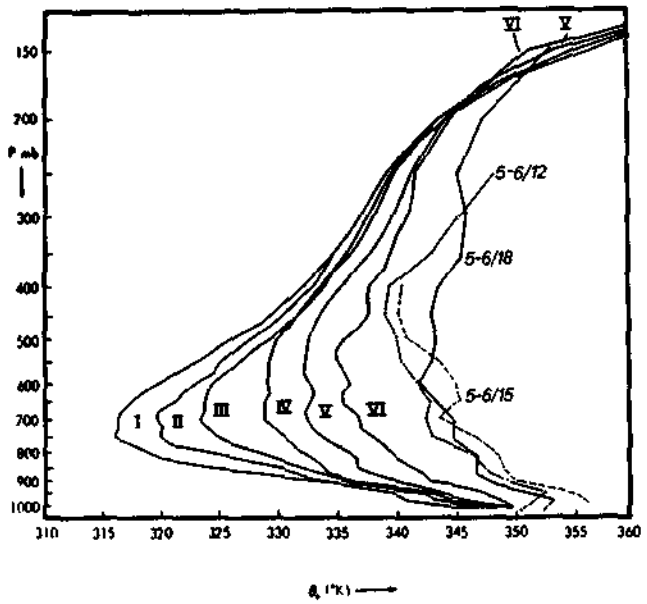

Fig. 15. Average equivalent potential temperature profiles calculated from the ABLE 2B network rawinsondes launched at 1200, 1500, and 1800 UT on May 6, 1987, added to θ_e profiles obtained from Barbados by *Aspliden* [1976]. The identifying numerals I–VI denote Aspliden's classification of energy in the tropical atmosphere from extremely depressed convection (I) containing only shallow cumulus clouds and no rainfall to severely enhanced convection (VI) characterized by cumulonimbi, several stratus decks, and heavy showers.

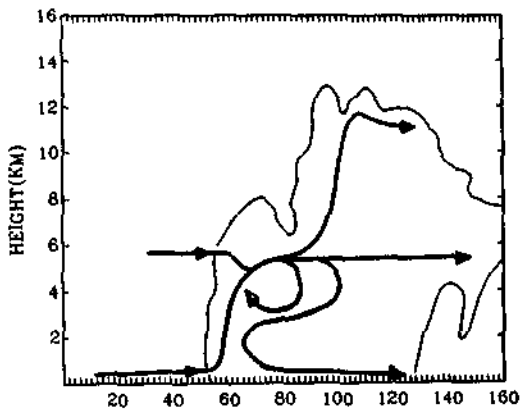

Fig. 16. Composite schematic of the predominant transport pathways for the May 6, 1987, model squall convection based on forward and backward trajectory analyses. The model cloud outline at 300-min simulation is included. The horizontal dimension is 80 km.

rather than the deeper tropospheric overturning evident in the dry season [*Garstang et al.*, 1988].

The passage of the May 6 squall line through the ABLE 2B network was marked by small thermodynamic modifications to the prestorm environment at three of the four PAM stations. Only Embrapa recorded a substantial gust front. At this location, the onset of convective precipitation (based on rain rate) occurred within minutes of the rapid drop in θ_e and was of short duration. Little rainfall of stratiform origin was observed. The model-predicted heating rates exhibited little cooling in the lowest 1 km of the troposphere from the evaporation of rain, resulting in a limited source of negatively buoyant air for the production of weak, local downdrafts at the model surface.

5.2. *Parcel Trajectory Analyses*

Sets of trajectories are calculated for specific grid points, levels, and elapsed time. This facilitates the interpretation of a 2-D flow pattern related to the character of tracer distribution by convective transports. The trajectories are computed backward and forward in time to illustrate particular features. Groups of points are chosen to illustrate particular features, but blocks of points are also used rather than a selection of systematic starting points to emphasize the organization and dispersion inherent in the cloud system on a scale larger than that of a single grid cell. Variables between grid points are estimated using a bicubic horizontal interpolation scheme with a linear interpolation in the vertical. The model-predicted wind fields are stored at 3-min intervals. A detailed discussion of the interpolation scheme and the parcel tracking algorithm can be found in the work by *Schlesinger* [1980].

Utilizing the model-generated wind fields, a series of forward and backward trajectory experiments are run to detail the predominant parcel pathways operating in the simulation. Parcel position relative to the squall convection is obtained by initially subtracting the modeled system's forward propagation. The trajectory calculations are performed systematically from left to right in the model domain. The calculations are performed from the surface to model top in three steps: low level (204–3072 m), midlevel (3506–8448 m), and upper level (9112–16128 m). The trajectories are computed over an elapsed time of 120 min (forward, 300–420; backward, 180–300).

The predominant pathways responsible for the majority of the transport through the model convection are depicted in Figure 16. Several distinct circulations producing multiple levels of detrainment are evident in the illustration. High θ_e air enters the core updraft at low levels in the leading edge of the system. Near-vertical ascent transports parcels to about 5.5 km. Interaction with the melting of frozen meteors at this level and an apparent flow through in the ambient wind field at 6 km prevents, at least initially, further ascent within the core updraft. All trajectories indicate horizontal displacement from the front of the cloud into the trailing stratiform region at this height before a second area of upward motion transports parcels to cloud top.

A shallow overturning downdraft originating at or below 2 km descends to the surface behind the core updraft. The cooling rates from the evaporation of raindrops are insufficient to support a strong outflow structure required to sustain a surface cool pool (Figure 14). Mesoscale downdrafts originating below the melting level induce a pronounced rotor at 4.5 km, similar to that found by *Tao and Simpson* [1989], but unlike the one contained within the density current of a multicell system [*Dudhia et al.*, 1987]. The clockwise circulation is maintained through the interaction of the core updraft and mesoscale sinking between 4 and 6 km.

The complexity of the transport pathways promote strong mixing within the system below 6 km, and between the cloudy air and the cloud-free environment. The primary regions of detrainment are in the anvil at 12 km, the midlevel at 6 km, and the wake outflow at the surface. Primary

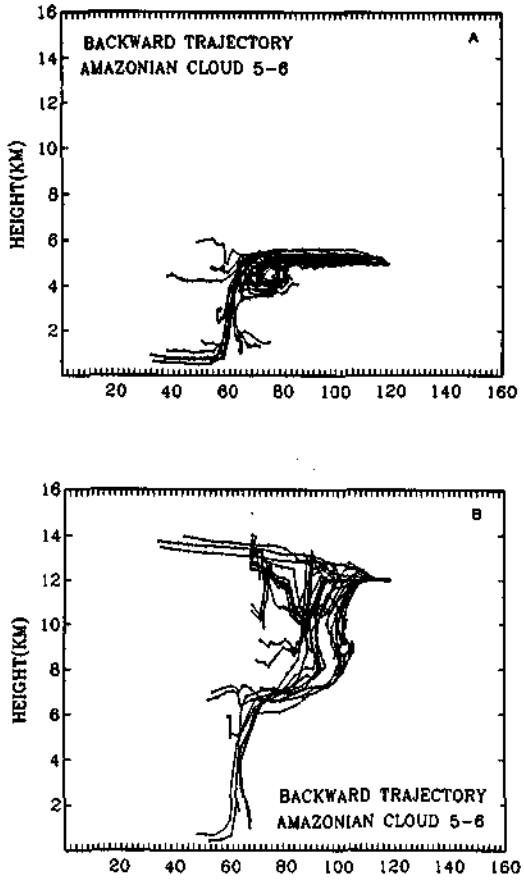

Fig. 17. Model-calculated backward trajectory paths during the time period 180–300 min. Each segment along a path represents movement during a 6-min time step. (*a*) Backward trajectory from a height of 4946 m showing interaction between the updraft and a pronounced rotor. (*b*) Backward trajectory from a height of 12 km showing the majority of parcels reaching this height originate from the middle and upper levels. The horizontal dimension is 80 km.

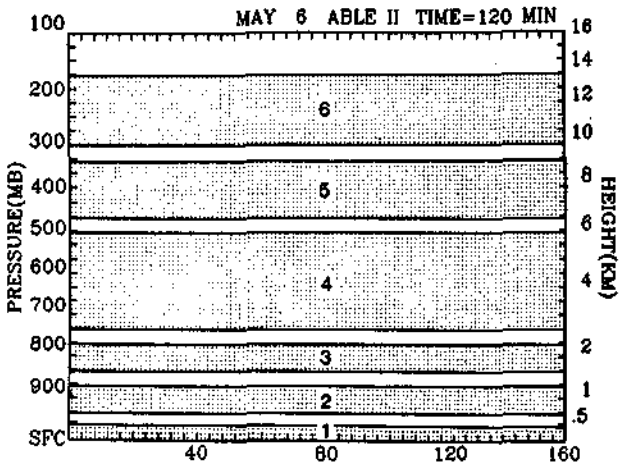

Fig. 18. The initial composite distribution of six inert tracer layers introduced into the simulation at 120 min. The vertical dimensions of each are tracer 1, 0.0–0.10 km; tracer 2, 0.31–0.81 km; tracer 3, 1.10–1.73 km; tracer 4, 2.09–5.21 km; tracer 5, 5.74–8.21 km; and tracer 6, 8.78–12.39 km.

entrainment occurs above the surface in the inflow region, the front inflow at 6 km (which may pass completely through the system), and a rotor centered at 4.5 km, where parcels may in theory detrain and entrain numerous times during the 120-min simulation.

The origins of air parcels involved in the midlevel rotor and those ascending to cloud top are identified using backward trajectories. Sets of 26 pathways representative of parcel transport within these circulations are presented in Figure 17. More than 50% of the trajectories terminating below 5 km become involved in the rotor at 4.5 km (Figure 17*a*). The rotor circulation appears critical to the dynamics of the modeled system because it impacts on air from the core updraft, from the midlevel inflow, and from mesoscale descent. Only about 15% of the air entering the core updrafts is transported directly to the cloud top near 12 km (Figure 17*b*). A substantial proportion (73%) of the parcels reaching the most active area of the anvil, the overshooting top, originate above 6 km. This result contrasts with the jump-type updrafts capable of transport from the lower to upper troposphere discussed by *Tao and Simpson* [1989].

5.3. *Tracer Studies*

A layered tracer scheme is used to investigate the transport efficiency of the modeled squall system and its effect on the vertical distribution of conservative trace gases; several simulations were conducted utilizing a layered tracer scheme. The advantage of this analysis is the tracer can be introduced at a specific time (e.g., at 120 min) in the simulation. Tracers are probably more accurate for determining the "origin" of air than trajectories, since the effects of subgrid scale diffusion are included and they do not involve interpolation between time intervals.

The inert tracers are introduced at different layers of varying depths based on the characteristics of a measured ozone profile obtained from Ducke at 1534 UT on May 6. Each layer requires a separate equation to calculate its change in concentration as a result of transport. The tracer is initialized to unity within each overlying layer, and zero elsewhere. The simulation is run for a specific forward time period similar to the trajectory analyses utilizing a 10-s time step. The model output is analyzed to determine the distribution of tracers and the effect of convective transports on their distribution. This technique is similar to the tracer analysis used by *Lafore and Moncrieff* [1989] to calculate the transport of three passive tracers. The selection of layers was based on the initial wind profile and the importance of these layers in the development of updraft and downdraft motions.

Six tracers are introduced into the model domain at 120-min simulation time (Figure 18). Each layer covered the horizontal extent of the model domain but varied considerably in thickness in an effort to accurately incorporate the measured vertical structure of ozone to a height of 12 km. After the 4-hour simulation, each tracer exhibited modification in response to the predominant vertical motions present in the simulated convection (Figure 19). The lowest layer, tracer 1, is influenced by weak vertical motions near the surface.

Upward transport of tracer 2 clearly delineates a near-vertical updraft to 5 km, with 40% of the initial concentration reaching 3.5 km. Downward transport results in concentrations also reaching 40% of their initial value to the surface, 40 km behind the updraft core. Nearly 80% dilution of this tracer occurs between these draft structures. The region of

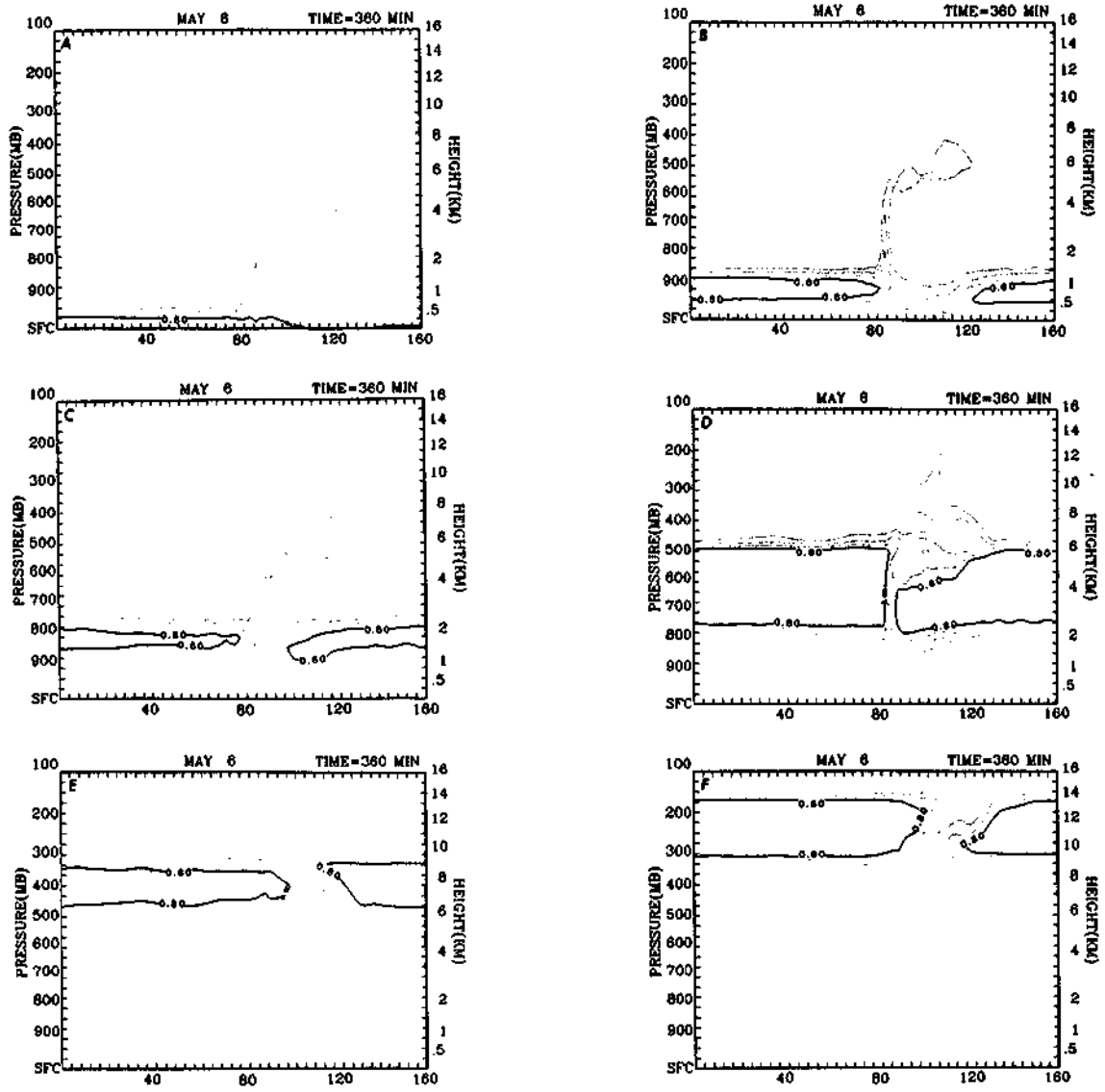

Fig. 19. The modification of the six tracers in Figure 18 by cloud transports after a simulation time of 240 min. Cloud model elapsed time is 360 min. The amount of tracer at each level is given as a percentage of its initial concentration (0.0–1.0). The contour interval is 0.2. (*a*) Tracer 1, (*b*) tracer 2, (*c*) tracer 3, (*d*) tracer 4, (*e*) tracer 5, and (*f*) tracer 6.

maximum mixing narrows to 20 km within tracer 3 (initially 1.1–1.7 km) after 4 hours of the simulation. The core updraft is evident but reduced in strength with concentrations of < 40% above 2.5 km. A rear overturning downdraft reinforcing the cold pool brings 20% air to within 200 m of the surface. Transport of tracer 4 (2.1–5.2 km) is characterized by an 8-km-wide core updraft to nearly 6 km. An additional weaker area of upward transport to cloud top corroborates the presence of vertical motion at this level seen in Figure 12. An apparent clockwise curvature to the vertical transport at 5.5 km, possibly demarcating the transition region between convective and stratiform processes, dilutes the initial tracer to 80% at 4 km.

The concentrations of tracer 5 (5.7–8.2 km) and tracer 6 (8.8–12.4 km) exhibit upward transport within the anvil region only. The weak structure evident within tracer 5 apparently originated in tracer 4, and is likely responsible for the overshooting top above 12 km. Maximum values of 40% reach to 14 km.

Modification of the model troposphere by propagating deep convection is demonstrated by the action of vertical drafts on inert tracers. Redistribution of the tracer field suggests mixing in the 1 to 2-km layer by nearly vertical updrafts, and relatively weak, penetrating downdrafts. Midlevel mixing confines the higher values of the tracer to the midtroposphere below 6 km, consistent with the trajectory estimates of limited deep transport. Undilute transport via convective updrafts to the anvil region is not indicated. The interaction of convective scale transports with the stratiform region at 5.5 km has important implications for tracer distributions, since both upward and downward motion may result following transport to this height.

6. PHOTOCHEMISTRY

The meteorological and chemical measurements taken onboard the Electra aircraft allow an assessment of the photochemistry occurring in the air in the vicinity of the May

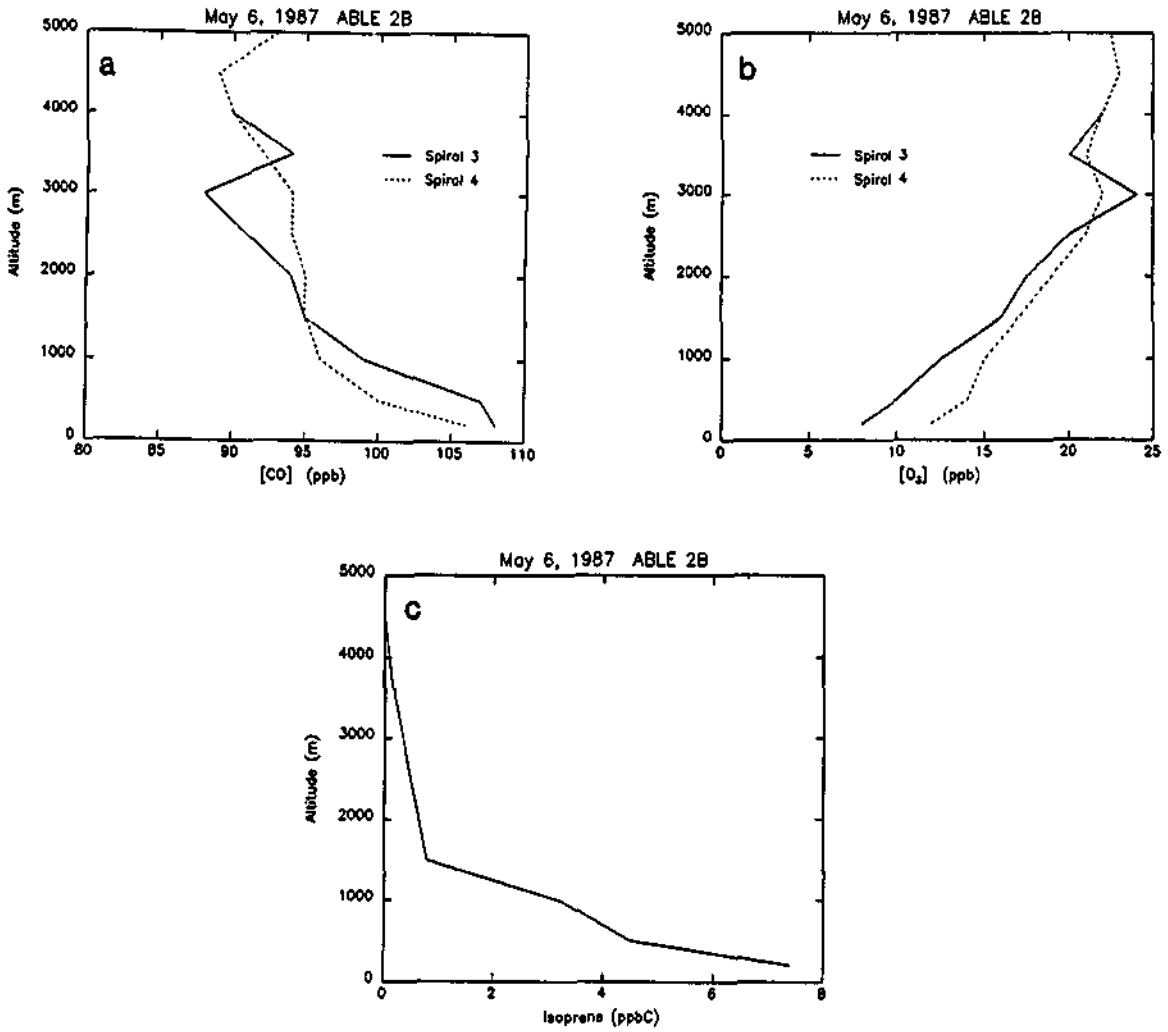

Fig. 20. Observed profiles of trace gases from the May 6, 1987, flight. The data were smoothed over 0.5-km intervals. (*a*) CO from spirals 3 and 4, (*b*) O_3 from spirals 3 and 4, and (*c*) isoprene from all samples obtained during the flight.

6 convective system. In particular, we examined the photochemical production of ozone in the air processed by the storm. Ozone production is examined for two reasons. First, convective systems can be very effective in redistributing trace gases which are ozone precursors. When NO is transported from source regions, it is spread over a larger volume, thereby becoming more dilute and more efficient in catalyzing ozone production [*Pickering et al.*, 1990; *Liu et al.*, 1987]. Second, we will determine if ozone can be considered a conservative tracer on the scale of this convective system. Ozone destruction is expected to dominate over ozone production because the NO concentrations are low (generally less than 10 ppt). The magnitude of the ozone loss rate in the May 6 case is determined by the concentrations of CO and water vapor [*Chameides et al.*, 1989]. Photochemical model calculations are necessary to estimate the magnitude of this ozone loss rate.

We selected as most appropriate for modeling those trace gas profiles obtained while the aircraft spiraled closest to the active convection. These are identified by using the results from the convective cloud model to evaluate whether the sampled air was likely to have been detrained from the convective system. At each model grid point the percentage of air arriving at that altitude from the cloud is estimated, and those altitude ranges where the majority of the air was cloud outflow are identified. Data from the outflow portions of spirals 3 (ahead of the system) and 4 and 5 (behind the system) are used to generate profiles for use in the photochemical model.

Measured profiles of CO and O_3 (smoothed to 0.5-km intervals) from spirals 3 (ahead) and 4 (behind) are shown in Figures 20*a* and 20*b*, respectively. Mixing in the lowest 3 km substantially reduced the vertical gradients of CO and O_3 behind the system compared with ahead of the squall line. Thirty-four samples for hydrocarbons were taken during the May 6 aircraft mission (R. A. Rasmussen and M. A. K. Khalil, unpublished data, 1989). Isoprene was the dominant species, both in terms of reactivity and concentration. The

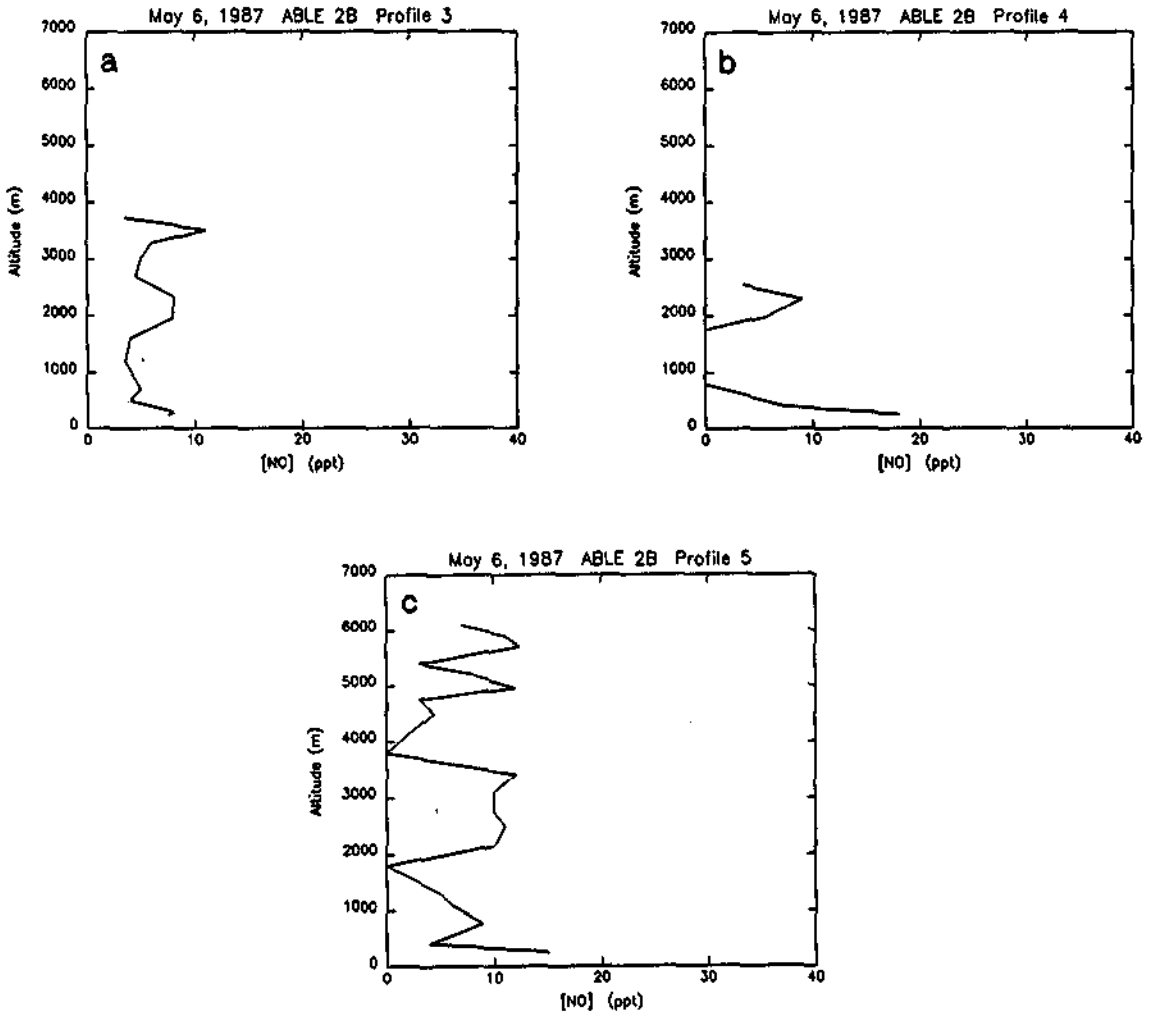

Fig. 21. Observed profiles of NO from the May 6, 1987, flight. The data were averaged over 1-min intervals. (*a*) Spiral 3, (*b*) spiral 4, and (*c*) spiral 5. Spirals 4 and 5 were obtained behind the squall line.

mean isoprene concentrations for the 0.5-km intervals are given in Figure 20*c*. Figure 21 shows the measured NO ahead of and behind the squall line. The data from spiral 5 (also behind the system) were included, since data from spiral 4 were only available to 2.5 km.

Ozone production for the detrained air below 5 km is evaluated with a one-dimensional photochemical model [*Thompson and Cicerone*, 1986]. The model contains 74 chemical reactions, including the oxidation of isoprene by OH. Full isoprene kinetics are not included, but a comparison of ozone production in the mixed layer for an ABLE 2A case using this method [*Pickering et al.*, 1989*a*] and that estimated by *Jacob and Wofsy* [1988] shows that the two estimates for undisturbed conditions are within 10%. A vertical grid of 24 altitude points between the surface and 11 km is used. The reaction rate coefficients are altitude dependent based on an observed temperature profile.

The net ozone production rate, $P(O_3)$, is computed using five rate terms representative of the rate-determining steps for the major production and loss mechanisms. $P(O_3)$ is calculated at 3-hour intervals over a 24-hour period following the convective event. Diurnally averaged production rates are also determined. The model is constrained using the observations of isoprene, CO, O_3, and water vapor to specify invariant profiles. The average flux of NO from soil measured during ABLE 2B [*Bakwin et al.*, this issue] is used to generate the NO profile in the model. Horizontal advection of lower or higher NO concentrations is simulated to match the NO observations.

The clear-sky photolysis rates are modified by the insertion of a slab cloud [*Thompson*, 1984] between 7 and 8 km to simulate the effects of an anvil cloud above the region being modeled. Inclusion of the cloud is necessary, since a stratiform deck persisted for several hours after the flight, reducing the radiation available for photolysis below the cloud. The cloud top albedo is assumed to be 0.6, representing approximately 3/4 cloud cover.

A comparison between the ozone production of air entering and exiting the storm could provide valuable information on cloud effects. However, the NO concentrations measured

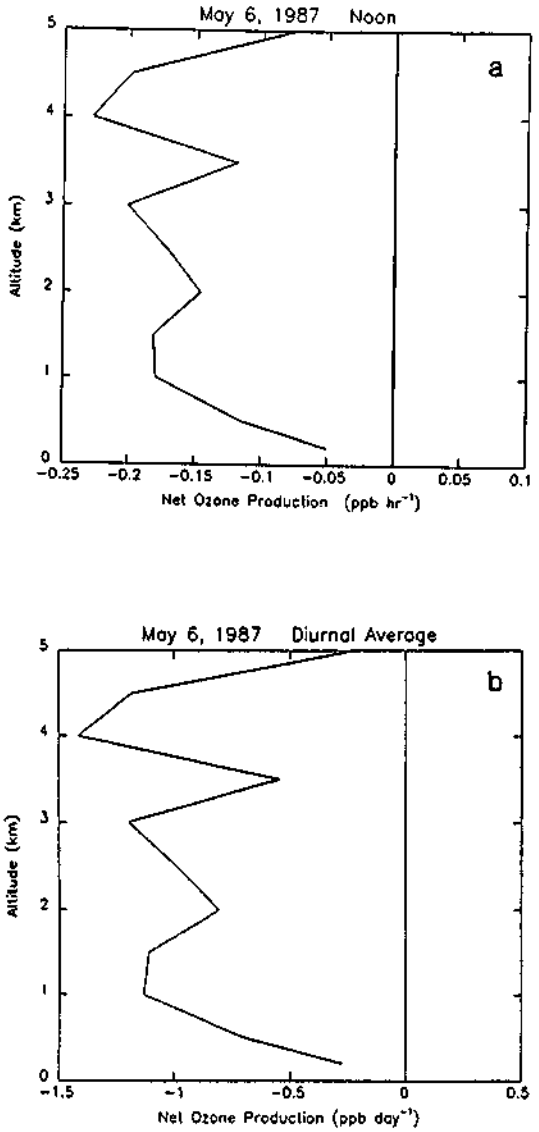

Fig. 22. Net ozone production rate as a function of altitude. (*a*) Noon local time (ppb h^{-1}) and (*b*) diurnally averaged (ppb d^{-1}).

during the May 6 flight were at or below the detection limit of the instrument for most of the mission, thus invalidating such a comparison. The photochemistry of relatively undisturbed boundary layer air during the wet season has been studied by *Jacob and Wofsy* [this issue]. Therefore the photochemical model is only run for the conditions present in the cloud-processed air.

The net ozone production estimates for the cloud processed air are presented in Figure 22. Photochemical destruction of ozone is computed for all altitudes between 0.2 and 5 km, both at noon and for the diurnal average. The results indicate the ratio of destruction is quite small, generally less than 0.2 ppb/h. These calculations suggest that ozone may be considered conservative under the wet season conditions of May 6 and for the time scale of the convection.

Excluding the 0.2-km results, ozone destruction rates in the cloud-processed air at noon are quite similar to those of *Jacob and Wofsy* [this issue]. Our calculated photochemical ozone loss in the mixed layer over a 25-hour period matches the Jacob and Wofsy estimate of 0.8 ppb. The ozone production results for this wet season convective system are in sharp contrast with those from a dry season convective case during ABLE 2A [*Pickering et al.*, 1989*a*] in which ozone production was estimated over nearly the entire altitude of measurement. Ozone precursors were available in larger concentrations in the dry season due to larger soil emission of NO and biomass burning.

7. Conclusions

Two-dimensional model calculations of trajectories through a simulated squall line observed during ABLE 2B exhibit evidence for regions of significant midlevel detrainment in addition to transports to anvil heights. The core updrafts appear to exit the main inflow as three distinct regions of motion: (1) a rotor circulation centered at 4.5 km, (2) a midtropospheric outflow at 6 km, and (3) an upperlevel outflow within an overshooting top directed to the rear of the storm.

Observational evidence supported by the cloud model results suggests the May 6 squall system resembled the unicell case presented by *Dudhia et al.* [1987]. Model-predicted column heating rates indicated little cooling in the low troposphere from the evaporation of rain. Without a sufficient source of negatively buoyant air, only weak, local downdrafts reached the cool pool at the model surface. Field observations obtained during storm passage also support a weak thermodynamic signature at the surface. The observed wind profile, crucial to the simulated system's structure, was quite similar to the unicell profile proposed by *Dudhia et al.* [1987].

Vertical profiles of ozone obtained by aircraft sampling on May 6 in the vicinity of deep convection reveal concentrations which are significantly lower than dry season estimates. Vertical gradients appear to be lacking in the presence of vigorous mixing of the lower troposphere. The presence of a low-level to midlevel rotor, suggested by the model trajectories may be responsible for this distinct vertical distribution.

One-dimensional photochemical model estimates of ozone destruction indicate a small daily ozone loss in the boundary layer. Thus changes in observed ozone concentrations in the lower troposphere appear to be dominated by convective transport rather than by photochemistry for the May 6 squall line. In this case, ozone can be considered a valid tracer of convective motion.

The results of this study suggest the *Riehl and Simpson* [1979] "hot tower" hypothesis, which describes deep undilute tropospheric transport over the tropical oceans as essentially closed conduits, may not apply to very moist continental tropical systems. The conduits appear to leak, and their physical description is likely time and cloud dependent. Undilute parcels that successfully reach anvil heights do so primarily because of rapid transport and avoidance of detrainment-entrainment pathways.

A significant portion of the air transported to anvil heights is drawn from the midtroposphere. Boundary layer air is subject to considerable mixing and modification prior to vertical transport through the column. The result of the marked middle and low tropospheric detrainment and recycling is to produce an extremely well-mixed atmosphere in the wake of deep convection. Only a small fraction of surface and boundary layer air, including trace gases and

particulates, is transported directly to the upper troposphere.

Much of the lower atmosphere is subject to rather rapid "parent cloud" entrainment-detrainment, and recycling. Part of the lower atmosphere is detrained and/or entrained from "cloud-to-cloud" interactions below 5.5 km. Lifetimes of boundary layer air parcels in clouds and in the near-cloud environment are therefore complex and difficult to determine. We believe, however, that a better understanding of both cloud chemistry and photochemical processes in concert with the transport of inert species is possible with careful model and observational studies of the kind presented here.

Acknowledgments. We gratefully acknowledge the broad support provided by the Tropospheric Chemistry Program of NASA in the GTE/ABLE experiments. Technical and scientific support has been generously provided by the NASA Goddard and Langley laboratories, and by the Electra flight crew and technicians of the Wallops Flight Facility. We thank two anonymous reviewers for suggestions that improved the content of this paper. The material presented in this paper forms part of J. Scala's doctoral dissertation submitted in partial fulfillment of that degree at the University of Virginia.

REFERENCES

Adler, R. F., and A. J. Negri, A satellite infrared technique to estimate tropical convective and stratiform rainfall, *J. Appl. Meteorol.*, *27*, 30–51, 1988.

Aspliden, C. I., A classification of the structure of the tropical atmosphere and related energy fluxes, *J. Appl. Meteorol.*, *15*, 692–697, 1976.

Auer, A. H., and J. D. Marwitz, Estimates of air and moisture flux into hailstorms on the high plains, *J. Appl. Meteorol.*, *7*, 196–198, 1968.

Bakwin, P. S., S. C. Wofsy, S. -M. Fan, M. Keller, S. Trumbore, and J. M. da Costa, Emission of nitric oxide (NO) from tropical forest soils and exchange of NO between the forest canopy and atmospheric boundary layers, *J. Geophys. Res.*, this issue.

Braham, R. R., The water and energy budgets of the thunderstorm and their relationship to thunderstorm development, *J. Meteorol.*, *9*, 227–242, 1952.

Browell, E. V., A. F. Carter, S. T. Shipley, R. J. Allen, C. F. Butler, M. N. Mayo, J. H. Siviter, and W. M. Hall, NASA multipurpose airborne DIAL system and measurement of ozone and aerosol profiles, *Appl. Opt.*, *22*, 522–534, 1983.

Brown, J. M., Mesoscale unsaturated downdraft driven by rainfall evaporation: A numerical study, *J. Atmos. Sci.*, *36*, 313–338, 1979.

Burpee, R. W., Peninsula-scale convergence in the south Florida sea breeze, *Mon. Weather Rev.*, *107*, 852–860, 1979.

Chameides, W. L., D. D. Davis, G. L. Gregory, G. Sachse, and A. L. Torres, Ozone precursors and ozone photochemistry over eastern North Pacific during the Spring 1984 based on NASA/GTE/CITE 1 airborne observations, *J. Geophys. Res.*, *94*, 9799–9809, 1989.

Charba, J., Application of gravity current model to analysis of squall-line gust front, *Mon. Weather Rev.*, *102*, 140–156, 1974.

Chatfield, R. B., and P. J. Crutzen, Sulfur dioxide in remote oceanic air: Cloud transport of reactive precursors, *J. Geophys. Res.*, *89*, 7111–7132, 1984.

Ching, J. K. S., and A. J. Alkezweeny, Tracer study of vertical exchange by cumulus clouds, *J. Clim. Appl. Meteorol.*, *25*, 1720–1711, 1986.

Cho, H. R., J. V. Iribarne, J. E. Grabenstetter, and Y. T. Yam, Effects of cumulus cloud systems on the vertical distribution of air pollutants, in *The Meteorology of Acid Deposition*, edited by P. J. Samson, pp. 127-139, Air Pollution Control Association, Pittsburg, Pa., 1984.

Cooper, H. J., M. Garstang, and J. Simpson, The diurnal interaction between convection and peninsula-scale forcing over south Florida, *Mon. Weather Rev.*, *110*, 486–503, 1982.

Dickerson, R. R., et al., Thunderstorms: An important mechanism in the transport of air pollutants, *Science*, *235*, 460–465, 1987.

Doneaud, A. A., S. Ionesco-Niscov, and J. R. Miller, Jr., Convective rain rates and their evolution during storms in a semi-arid climate, *Mon. Weather Rev.*, *112*, 1602–1612, 1984.

Dudhia, J., M. W. Moncrieff, and D. W. K. So, The two-dimensional dynamics of West African squall lines, *Q. J. R. Meteorol. Soc.*, *113*, 121–146, 1987.

Echternacht, K. L., and M. Garstang, Changes in the structure of the tropical subcloud layer from the undisturbed to disturbed states, *Mon. Weather Rev.*, *104*, 407–417, 1976.

Fankhauser, J. C., Estimates of thunderstorm precipitation efficiency from field measurements in CCOPE, *Mon. Weather Rev.*, *116*, 663–684, 1988.

Fitzjarrald, D. R., B. L. Stormwind, G. Fisch, and O. M. R. Cabral, Turbulent transport observed just above the Amazon forest, *J. Geophys. Res.*, *93*, 1551–1563, 1988.

Foote, G. B., and J. C. Fankhauser, Airflow and moisture budget beneath a northeast Colorado hailstorm. *J. Appl. Clim.*, *12*, 1330–1353, 1973.

Fovell, R. G., and Y. Ogura, Numerical simulation of a mid-latitude squall line in two dimensions, *J. Atmos. Sci.*, *45*, 3846–3879, 1988.

Gamache, J. F., and R. A. Houze, Jr., Mesoscale air motions associated with a tropical squall line, *Mon. Weather Rev.*, *110*, 118–135, 1982.

Garstang, M., et al., Trace gas exchanges and convective transports over the Amazonian rain forest, *J. Geophys. Res.*, *93*, 1528–1550, 1988.

Garstang, M., et al., The Amazon Boundary Layer Experiment (ABLE 2B): A meteorological perspective, *Bull. Am. Meteorol. Soc.*, *71*, 19–32, 1989.

Gidel, L. T., Cumulus cloud transport of transient tracers, *J. Geophys. Res.*, *88*, 6587–6599, 1983.

Greenhut, G. K., Transport of ozone between boundary layer and cloud layer by cumulus clouds, *J. Geophys. Res.*, *91*, 8613–8622, 1986.

Hane, C. E., The squall line thunderstorm: Numerical experimentation, *J. Atmos. Sci.*, *30*, 1672–1690, 1973.

Harriss, R. C., et al., The Amazon Boundary Layer Experiment (ABLE 2A): Dry season 1985, *J. Geophys. Res.*, *93*, 1351–1360, 1988.

Jacob, D. J., and S. C. Wofsy, Photochemistry of biogenic emissions over the Amazon forest, *J. Geophys. Res.*, *93*, 1477–1486, 1988.

Jacob, D. J., and S. C. Wofsy, Budgets of reactive nitrogen, hydrocarbons, and ozone over the Amazon forest during the wet season, *J. Geophys. Res.*, this issue.

Johnson, R. H., The role of convective-scale precipitation downdrafts in cumulus and synoptic scale interaction, *J. Atmos. Sci.*, *33*, 1890–1910, 1976.

Kirchhoff, V. W. J. H., I. M. O. da Silva, and E. V. Browell, Ozone measurements in Amazonia: Dry season versus wet season, *J. Geophys. Res.*, this issue.

Klemp, J. B., and R. B. Wilhelmson, The simulation of three-dimensional convective storm dynamics, *J. Atmos. Sci.*, *35*, 1070–1096, 1978.

Knupp, K. R., Downdrafts within High Plains cumulonimbi, I, General kinematic structure. *J. Atmos. Sci.*, *44*, 987–1008, 1987.

Lafore, J. -P., and M. W. Moncrieff, A numerical investigation of the organization and interaction of the convective and stratiform regions of tropical squall lines, *J. Atmos. Sci.*, *46*, 521–544, 1989.

Liu, S. C., M. Trainer, F. C. Fehsenfeld, D. D. Parrish, E. J. Williams, D. W. Fahey, G. Huebler, and P. C. Murphy, Ozone production in the rural troposphere and the implications for regional and global ozone distributions, *J. Geophys. Res.*, *92*, 4191–4207, 1987.

Lyons, W. A., R. H. Calby, and C. S. Keen, The impact of mesoscale convective systems on regional visibility and oxidant distribution during persistent elevated pollution episodes, *J. Clim. Appl. Meteorol.*, *25*, 1518–1531, 1986.

Mahoney, W. P., Gust front characteristics and the kinematics associated with interacting thunderstorm outflows, *Mon. Weather Rev.*, *116*, 1474–1491, 1988.

Miller, L. J., J. D. Tuttle, and C. A. Knight, Airflow and hail growth

in a severe northern High Plains supercell, *J. Atmos. Sci.*, *45*, 736–762, 1988.

Moncrieff, M. W., The dynamical structure of two-dimensional steady convection in constant vertical shear, *Q. J. R. Meteorol. Soc.*, *104*, 336–352, 1978.

Moncrieff, M. W., Dynamical models of the transport of momentum, mass and inert tracers by mesoscale convective systems, paper presented at Symposium on the Role of Clouds in Atmospheric Chemistry and Global Climate, Am. Meteorol. Soc., Anaheim, Calif., Jan. 30 to Feb. 3, 1989.

Moncrieff, M. W., and M. J. Miller, The dynamics and simulation of tropical cumulonimbus and squall lines, *Q. J. R. Meteorol. Soc.*, *102*, 373–394, 1976.

Newton, C. W., Circulations in large sheared cumulonimbus, *Tellus*, *4*, 699–712, 1966.

Nicholls, M. E., A comparison of the results of a two-dimensional numerical simulation of a tropical squall line with observations, *Mon. Weather Rev.*, *115*, 3055–3077, 1987.

Nicholls, M. E., and M. J. Weissbluth, A comparison of two-dimensional and quasi-three-dimensional simulations of a tropical squall line, *Mon. Weather Rev.*, *116*, 2437–2452, 1988.

Nicholls, M. E., R. H. Johnson, and W. R. Cotton, The sensitivity of two-dimensional simulations of tropical squall lines to environmental profiles, *J. Atmos. Sci.*, *45*, 3625–3649, 1988.

Pickering, K. E., A. M. Thompson, and R. R. Dickerson, Model estimates of enhanced photochemical production of ozone resulting from convective transport of precursors, paper presented at Symposium on the Role of Clouds in Atmospheric Chemistry and Global Climate, Am. Meteorol. Soc., Anaheim, Calif., Jan. 30 to Feb. 3, 1989*a*.

Pickering, K. E., A. M. Thompson, W. -K. Tao, M. Garstang, and R. C. Harriss, Net ozone production in air processed by tropical convective clouds, *Eos Trans. AGU*, *70*, 288, 1989*b*.

Pickering, K. E., A. M. Thompson, R. R. Dickerson, W. T. Luke, D. P. McNamara, J. P. Greenberg, and P. R. Zimmerman, Model calculations of tropospheric ozone production potential following observed convective events, *J. Geophys. Res.*, in press, 1990.

Raymond, D. J., A. M. Blyth, and O. Sanchez, Vertical transports by cumulus clouds—Recent results, paper presented at Symposium on the Role of Clouds in Atmospheric Chemistry and Global Climate, Am. Meteorol. Soc., Anaheim, Calif., Jan. 30 to Feb. 3, 1989.

Riehl, H., and J. Simpson, The heat balance of the equatorial trough zone, revisited, *Beitr. Phys. Atmos.*, *52*, 287–305, 1979.

Schlesinger, R. E., A numerical model of deep moist convection, II, A prototype experiment and variations on it, *J. Atmos. Sci.*, *30*, 1374–1391, 1973.

Schlesinger, R. E., A three-dimensional numerical model of an isolated deep thunderstorm, II, Dynamics of updraft splitting and mesovortex couplet evolution, *J. Atmos. Sci.*, *37*, 395–420, 1980.

Seitter, K. L., and H. -L. Kuo, The dynamical structure of squall-line type thunderstorms, *J. Atmos. Sci.*, *40*, 2831–2854, 1983.

Soong, S. -T., and Y. Ogura, Response of trade-wind cumuli to large-scale processes, *J. Atmos. Sci.*, *37*, 2035–2050, 1980.

Soong, S. -T., and W. -K. Tao, Response of deep tropical clouds to mesoscale processes, *J. Atmos. Sci.*, *37*, 2016–2034, 1980.

Tao, W. -K., and J. Simpson, Modeling study of a tropical squall-type convective line, *J. Atmos. Sci.*, *46*, 177–202, 1989.

Tao, W. -K., and S. -T. Soong, The study of the response of deep tropical clouds to mesoscale processes: Three-dimensional numerical experiments, *J. Atmos. Sci.*, *43*, 2653–2676, 1986.

Thompson, A. M., The effect of clouds on photolysis rates and ozone formation in the unpolluted troposphere, *J. Geophys. Res.*, *89*, 1341–1349, 1984.

Thompson, A. M., and R. J. Cicerone, Possible perturbations to atmospheric CO, CH_4, and OH, *J. Geophys. Res.*, *91*, 10,853–10,864, 1986.

Ulanski, S. L., and M. Garstang, The role of surface divergence and vorticity in the life cycle of convective rainfall, I, Observation and analysis, *J. Atmos. Sci.*, *35*, 1047–1062, 1978.

Wakimoto, R. M., The life cycle of thunderstorm gust fronts as viewed with Doppler radar and rawinsonde data, *Mon. Weather Rev.*, *110*, 1060–1082, 1982.

Watson, A. I., R. L. Holle, J. B. Cunning, P. T. Gannon, and D. O. Blanchard, Low-level convergence and the prediction of convective precipitation in south Florida, *Tech. Rep. 4*, 288 pp., Office of Weather Res. and Modification, NOAA/ERL, Boulder, Colo., 1981.

Weisman, M. L., J. B. Klemp, and R. Rotunno, Structure and evolution of numerically simulated squall lines, *J. Atmos. Sci.*, *45*, 1990–2013, 1988.

Zipser, E. J., The role of organized unsaturated convective downdrafts in the structure and decay of an equatorial disturbance, *J. Appl. Meteorol.*, *8*, 799–814, 1969.

Zipser, E. J., Mesoscale and convective-scale downdrafts as distinct components of squall line structure, *Mon. Weather Rev.*, *105*, 1568–1589, 1977.

E. V. Browell, G. L. Gregory, and G. W. Sachse, NASA Langley Research Center, Hampton, VA 23665.

M. Garstang, Department of Environmental Sciences, Clark Hall, University of Virginia, Charlottesville, VA 22903.

M. A. K. Khalil and R. A. Rasmussen, Institute of Atmospheric Sciences, Oregon Graduate Center, Beaverton, OR 97006.

V. W. J. H. Kirchhoff, Instituto de Pesquisas Espaciais, Caixa Postal 515, 12201-São José dos Campos, São Paulo, Brazil.

K. E. Pickering, Applied Research Corporation, Landover, MD 20785.

J. Scala, J. Simpson, W. -K. Tao, and A. M. Thompson, Laboratory for Atmospheres, NASA Goddard Space Flight Center, Greenbelt, MD 20771.

A. L. Torres, NASA Wallops Flight Facility, Wallops Island, VA 23337.

(Received August 8, 1989;
revised March 8, 1990;
accepted March 8, 1990.)